JOURNAL OF MECHANICAL ENGINEERING AND SCIENCES
ISSN: 2289-4659 e-ISSN: 2231-8380
VOLUME 17, ISSUE 4, 2023, 9791 – 9810
DOI: https://doi.org/10.15282/jmes.17.4.2023.11.0775

UNIVERSITI MALAYSIA PAHANG AL-SULTAN ABDULLAH

RESEARCH ARTICLE

Development of hydrophobic coating on 3D printed ABS samples and surface characterization

Y.S. Narayan*, P. Satyanarayana, K. J. Prakash and P. Narendra

Department of Mechanical Engineering, VNR Vignana Jyothi Institute of Engineering and Technology, Hyderabad, 500090, Telangana, India
Phone: +91 9849272656; Fax: +91 040 23042761

ABSTRACT - Manufacturers are increasingly substituting additive manufacturing for conventional manufacturing methods due to their ability to produce complex shapes. Polymer-based filament materials can be printed efficiently and inexpensively with fused deposition modeling. Coatings tend to augment the appearance of 3D printed objects as well as protect them from environmental influences. It is imperative to realize the physical and chemical properties of polymeric material like Acrylonitrile Butadiene Styrene (ABS) surfaces so as to design an optimal surface system. This work relates to the development of surface coatings on 3D-printed ABS parts. L9 orthogonal array was used with three 2 level factors for printing the samples. Specifically, the research compares surface characteristics of 3D-printed uncoated and coated ABS specimens. An aqueous solution containing Tricalcium phosphate and Chitin clear solutions in a 70:30 ratio was applied through immersion technique to create hydrophobic coatings. The coated and uncoated samples were characterized by employing various characterization tests, including dimensional accuracy (DA), surface roughness (SR), water contact angle (WCA), absorbency tests, scanning electron microscopy on fabricated parts. Assessment of wettability of 3D printed samples and impact of coating was accomplished via static contact angle measurements. In order to assess DA and SR before and after coating, digital vernier calipers were used in conjunction with a profilometer. In accordance with ASTM D570-98, water absorption tests were conducted for specified time. Results of investigation post coating showed no variation in dimensional accuracy, reduced SR and increased in WCA by ≥ 100˚. A reduction in water retention was observed after coating based on water absorption tests.

ARTICLE HISTORY
Received : 22nd May 2023
Revised : 06th Oct. 2023
Accepted : 20th Nov. 2023
Published : 26th Dec. 2023

KEYWORDS
3D printing
Hydrophobic surface
Dimensional accuracy
Surface roughness
Water contact angle
Absorption test

1.0 INTRODUCTION

In additive manufacturing (AM), layers of material are placed in succession via computer control in order to create a 3D object of desired form [1]. Printing complex structures at fine resolution have been made possible through additive manufacturing. Fused deposition modelling (FDM) mainly uses polymer filaments [2]. For fast prototyping, polymers have been the most commonly used. As a mechanical support for medical implants and inert materials, polymers have played an important role in developing biomaterials and medical devices [3]. Many materials have been created to increase the functioning of 3D printers, including acrylonitrile butadiene styrene (ABS), polylactic acid (PLA), high impact polystyrene, thermoplastic polyurethane, and aliphatic polyamides (nylon). Moreover, 3D printers can utilize natural fibers, which are biodegradable and have better properties [4]. A dimensional accuracy study was done using ABS and PLA specimens fabricated at different layer thickness (LT), raster angle (RA), and building orientations using the fused deposition modelling process [5]. Z-ABS dimensional accuracy was examined on the basis of sample size, LT and infill density. As a result of the 'size effect', sample's real dimensions are altered, usually observed during mechanical characterization [6]. A wax-coating and a Ni-Co-Cr alloy coating are effective in improving ABS's properties [7]. By coating polymers with graphene, tribological properties can be enhanced [8]. An alkali wet chemical can generate PLA surfaces after one hour (1 hour AT) or after six hours (6 hours AT), then nano hydroxyapatite (nHA) is added [9]. The biocompatible polyvinylpyrrolidone hydrogels were prepared by coating PLA flat discs and 3D-printed scaffolds with nHA [10]. ABS material can be chemically finished with acetone and hot air, while smooth surfaces can be treated with acetone [11, 12].

Roughness of specimens was enhanced by using solvents such as acetone, esters, and chlorides [13]. An XTC-3D coating was used to assess the finish on 3D printed objects [14]. During 3D printing, fillet radius of the specimen and printer settings influence the amount of material deposited [15]. CO2 laser scanning was used to optimize FDM printed ABS and PLA polymers [16]. By using cold vapor of dimethyl ketone on ABS parts, the surface quality was significantly improved [17, 18]. In conjunction with mechanical abrasion pre-treatment, wettability on the surface increases with surface energy (SE). With the increase of the normal force acting on the system [19], a higher value of surface roughness, R_a obtained for the abraded specimens. In order to fabricate micro or nanoscale surface structures utilizing hydrophobic materials, laser surface ablation and mechanical machining have been used. There are several methods for depositing

***CORRESPONDING AUTHOR | Y. S. Narayan** | ✉ shivrajyeole@vnrvjiet.in

hydrophobic coatings, including electrochemical deposition, chemical etching, photolithography, sputtering, phase segregation, sol-gelling, self-assembling and electrospinning. In addition to being time-consuming and expensive, these methods are also labour-intensive [20]. Nanoceramic resin coated with GF-2200 hydrophobic coating has a maximum angle of 110° at ambient temperature[4]. In order to create a super-hydrophobic composite coating [21], ACNTB-Sio_2 - KH570 was combined with epoxy (EP) adhesive precursor. Layered deposition components with hydrophobic coatings containing silica nanoparticles and MEK are less affected by surface coatings [22].

Dimensional accuracy was determined by comparing the printed specimens with a CAD model. Vernier callipers were used to measure three points. Compared to ABS, PLA, PP, and PET, all four materials showed greater precision along X and Y axes dimensions, while an FDM model provides real dimensions [23]. The exact dimensions of the samples were determined by averaging actual dimensions. In accordance with ASTM D570-98, PLA specimens were tested for water absorption. There was a significant increase in moisture consumption by the LVL1 (Level 1) sample despite the presence of protective coatings, whether they are applied or not [24]. There are several printing characteristics that can affect DA, such as shells, print temperature, infill, and printing style [25, 26]. $C_{10}H_{30}O_5Si_5$, SiO_2 nanoparticles (R812S), $(C_2H_6OSi)_n$ (BP-9400) and a non-ionic surface-active agent are included in this combination (Triton X-100). An increase in water contact angle was observed when a modified varnish with a weight percentage of modifying agents larger than 101.87 percent was applied to a Pineapple peel fiber (PAPF) bio composite [27]. The accuracy of samples could be decreased by long-term dimensional instability. The accuracy of samples could be decreased by long-term dimensional instability. Less than 0.1% of the dimensions varied. However, moisture absorption contributed to dimensional uncertainty for some polymers, such as polyamides [28]. Using an inductively coupled plasma (ICP) treatment followed by deposition of plasma based on fluorocarbon, surface hydrophobicity was modified on polymer blend surfaces [29].

The chitin hydrogels made with 3% LiCl had a low viscosity and exhibited a viscous behaviour. Accumulation of chitin segments on surface of hydrogel resulted in soft structure and poor mechanical traits in hydrogels formulated with 10% LiCl [30]. Superhydrophobic surfaces were created by spray coating silicon wafers with chitosan nanoparticles [31]. Ca-O-P gel was applied in layers 1 and 5 to a substrate coated with the gel, resulting in a higher CA ranging between 77-79°. Highest CA of 87° was attained in specimen after 15 dips. CA of the surface decreased to 75° after 30 dips [32]. A contact angle of more than 160 degrees was achieved in all microchannel surfaces coated with TiO2-HTMS. Any type of material can be coated with plasma polymerized coatings and topographies imparting hydrophobicity or super hydrophobicity [33, 34]. These layers of hydrogel/CP coating contain hydroxyapatite, brushite, octa calcium phosphate, and hydroxyapatite [35]. As PLA's external surfaces degrade, the absorption rates may change rapidly due to its organic nature [36]. Chemicals such as Ag, fluorine and saline chemicals containing compounds are commonly found in these coatings, which are hazardous to the environment and expensive. Hydrophobic coatings with smart, responsive properties have become an inevitable trend due to their low cost and eco-friendliness. To determine surface wettability and water absorption, various chemical concentrations must be studied prior to applying coatings to printed items. Among the best functional materials, chitin and tricalcium phosphate have excellent biocompatibility, biodegradability, and nontoxicity.

Current research compares surface characterization on coated and uncoated 3D printed samples under different process parameters. The main objective is to develop a hydrophobic surface coating on 3D printed samples such that they are light in weight, cheap to manufacture and comfortable for use. In this investigation, three different samples of ABS material were produced using 3D-printed FDM technology. L9 OA based Design of Experiments (DOE) employing 3 levels of two factors i.e., layer height and infill percentage were employed. Two replicates of samples 'R_1' and 'R_2', were obtained. R_2 samples were coated using immersion technique. The coatings were synthesized to acquire hydrophobic surfaces by combining tricalcium phosphate and Chitin clear solutions with a 70:30 ratio. An investigation was conducted on uncoated (R_1) and coated (R_2) samples to evaluate the surface characterization such as DA, SR, Scanning Electron Microscope (SEM), WCA and water absorption (WA) tests. To evaluate SR and DA, roughness measuring profilometer and digital vernier callipers were used. To verify whether the surfaces of coated and uncoated samples are in hydrophobic or hydrophilic conditions, WCA test was performed using a droplet contact angle measuring instrument. Water absorption tests were performed as per ASTM D570.

2.0 MATERIALS AND METHOD

All tests were executed on surfaces of ABS (3D printer Filament) samples. For the synthesis of solutions and coating, following were used – Chitin purified, Tricalcium phosphate extra purified (MW= 310.18 g mol^{-1}) [Manufacturer: OTTO]; HCL [99%], Acetic Acid [99%], Sulfuric acid, NaOH [in pallets], DMAc, LiCl, isopropyl alcohol, MEK [Manufacturer: SDFCL (SD Fine Chemical Limited)].

2.1 Design of Samples

A 3D models of BCC structure, square block with hexagonal filing and top and bottom plate along the structure were modelled in CATIA software as depicted in Figure 1 and converted into STL files. Sample identification is shown in Table 1. Dimensions of sample 1 are 31 x 31 x 5 mm with square holes of 1 x 1 mm. Sample 2 has dimensions of 31 x 31 x 5 mm and sample 3 has dimensions of 31 x 31 x 5 mm with square holes of 1 x 1 mm and plates of 31 x 31 x 1 mm.

Table 1. Identification of samples

3D Printed Specimens	Samples
BCC structure	1
Square block with hexagonal filling	2
Top and bottom plate along the structure	3

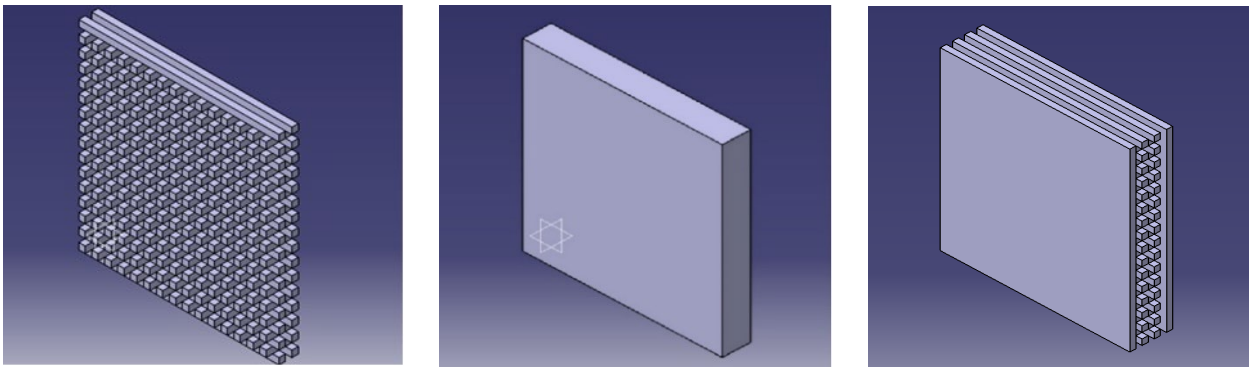

(a) (b) (c)

Figure 1. 3D CAD models: (a) BCC structure, (b) square block and (c) BCC structure with top and bottom plates

2.2 Design of Experiments

MINITAB software was utilized in design of experiment. $L_9(3^4)$ orthogonal array allows two 3-level factors to be studied along with an interaction. As layer height and infill percentage have been found to influence the surface characteristics in the case of 3D printed material and applications [35], it was decided to study interaction among layer height and infill percentage as a parameter with 3-layer thicknesses (in mm) and 3-infill percentages (%) as exhibited in Table 2.

Table 2. Input variables

Factors	Level 1	Level 2	Level 3
Layer height (mm)	0.15	0.17	0.20
Infill (%)	0	20	30

A and B represent variables of layer height (in mm) and infill (%), respectively, which are mapped to the first two columns of OA. Two replicates were planned to be performed on each test resulting in a total of 18 samples. Replicate R_1 indicate samples before applying the coating whereas replicate R_2 indicate samples after coating. Table 3 shows experimental design for L9 OA. Digits 1, 2, and 3 in columns R_1 and R_2 depict identification of samples as exhibited in Figure 1 and Table 1, respectively.

Table 3. Mapping of factor levels to OA

S.No.	A	B	R_1	R_2
1	0.15	0	1	1
2	0.15	20	2	2
3	0.15	30	3	3
4	0.17	0	1	1
5	0.17	20	2	2
6	0.17	30	3	3
7	0.20	0	1	1
8	0.20	20	2	2
9	0.20	30	3	3

2.3 Fabrication of Samples in FDM 3D Printer

A flash forge dreamer 3D printer based on FDM technology was used to print the test specimens as shown in Figure 2(a) and working of FDM printer is shown in Figure 2(b). Sliced STL model was obtained in Flash print software. Table 4 illustrates characteristics of ABS material. Specimens were printed under R_1 and R_2 categories according to parameters shown in Table 5 and exhibited in Figure 3. Post-processing involved removing dust and other contaminants with concentrated isopropyl alcohol after printing.

Table 4. Characteristics of ABS material

Material	ABS	Color	Black
Brand	3D printed filament	Density	1.04 g/cm^3
Diameter	1.75 mm	Printing temperature	220-250 °C
Melting point temperature	220 °C	Flow rate	2-4g/10 min

Table 5. Printing parameters

S. No.	A	B	R_1	R_2	Infill Type	No. of Shells
1	0.15	0	1	1	-	2
2	0.15	20	2	2	Hexagonal	2
3	0.15	30	3	3	Hexagonal	2
4	0.17	0	1	1	-	2
5	0.17	20	2	2	Hexagonal	2
6	0.17	30	3	3	Hexagonal	2
7	0.20	0	1	1	-	2
8	0.20	20	2	2	Hexagonal	2
9	0.20	30	3	3	Hexagonal	2

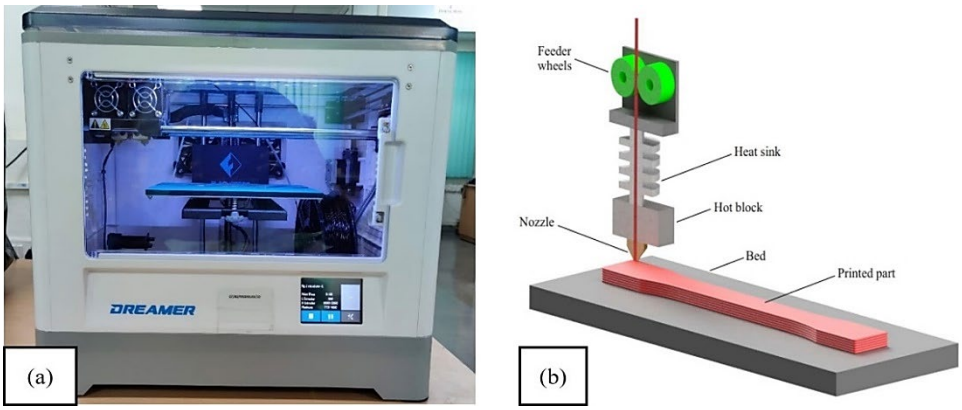

Figure 2. FDM printing: (a) Dreamer printer and (b) working principle

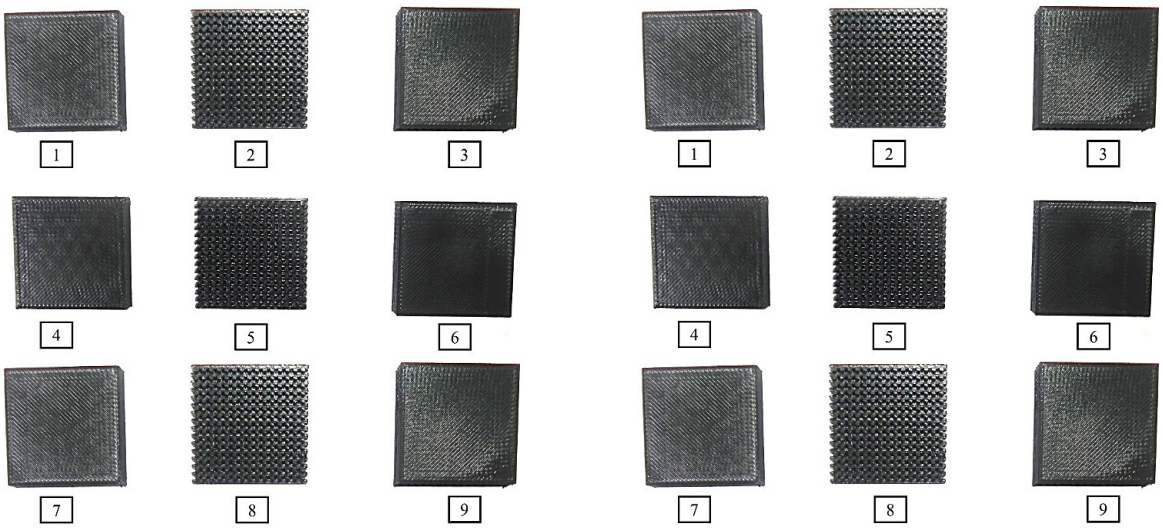

Figure 3. 3D printed samples: (a) R_1 and (b) R_2

2.4 Synthesis of Surface Coatings

2.4.1 Preparation of Tricalcium Phosphate solution

Surface coatings were produced by a concoction of Tricalcium phosphate-chitin solutions with ratios of 70:30. Table 6 displays chemical proportions of tricalcium phosphate. Solution 1 was prepared by adding 4 g of tricalcium phosphate, 6 ml HCL and made up to 100 ml in the beaker. At room temperature, this mixture was blended for 30 minutes at 1600 rpm. The process was repeated for making another 100 ml tricalcium phosphate solution. Solution was observed to be clear after 24 hours which is designated as A_1.

Table 6. Tricalcium phosphate solution chemical quantities

Solution	Tricalcium Phosphate (g)	HCL (ml)	Distilled Water (ml)	No. of Samples
A_1	4	6	96	2

2.4.2 Preparation of Chitin solution

Table 7 displays chemical quantities of Chitin solution**.** Solution 2 was prepared by adding 1.5 g of Chitin to 7.5 g of LiCl of 150 ml DMAc to that 150 ml of MEK in to the beaker. The solution was blended at room temperature for 3 hours at 1600 rpm. After 24 hours, the mixture was centrifugated for 10 minutes at 2500 rpm to remove precipitates, and a clear solution was observed which is designated as B_1.

Table 7. Chitin solution chemical proportions

Solution	$(C_8H_{13}O_5N)_n$ (g)	LiCl (g)	DMAc (ml)	MEK (ml)	No. of samples
B_1	1.5	7.5	150	150	1

Table 8 shows chemical quantities used for preparation of 80 ml solution of 70:30 ratios. The solutions were stirred for 10 minutes at 2500 rpm using a magnetic stirrer at room temperature.

Table 8. Tricalcium phosphate-chitin solution concentration proportions

Solution	Composition of Tricalcium phosphate – chitin solution	Ratios
S1	A_1:B_1	
S2	A_1:B_1	56:24
S3	A_1:B_1	

2.5 pH Level Measurement

An Elico LI 120 pH meter was used to measure pH level of surface coating solution. Initially, pH level of the solution was 1.2. For hydrophobic surfaces, the pH level must be 7 or higher [33]. To make the pH level 7, titration process was used with 5M (5 Moles) of NaOH solution added slowly until the pH level reach 7. pH level dropped rapidly with addition of NaOH solution. After 24 hours, the solution was centrifugated at 2500 rpm for 10 minutes. Consequently, a clear solution was reached. The precipitates were appended to 100 ml distilled water and mixed, followed by addition of phenolphthalein. The solution turned pink, indicating that the precipitates are NaOH. The pH of the solution was 8 after titration and crossed 7 after day 2. An illustration of the difference in pH level responses before and after adding aqueous NaOH can be found in Table 9**.** Graphs of pH level responses for day-to-day variations in solutions are exhibited in Figure 4. Initially, pH values of solution are 1.12 indicating its acidic nature. After the titration process, pH value increased to 8.0 indicating its alkaline nature. After the centrifugation process, pH level stabilized at 7.20 from day 2 to day 4 respectively indicating its neutral nature.

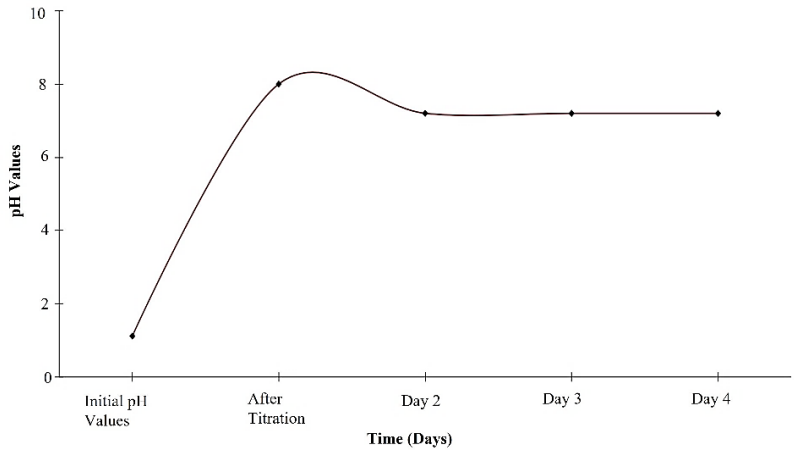

Figure 4. Variations in pH level responses in solutions

2.6 Coating of 3D Printed Samples

R_2 3D printed specimens were immersed in the synthesized solution for application of coating. 3D-printed samples were dip coated for 60 minutes followed by drying at room temperature for period of 24 hours. Table 9 gives the mapping of 3D printed specimens and their immersing solutions**,** whereas Figure 5 shows the immersion process.

Table 9. 3D printed R_2 specimens are immersed in solutions

Solutions	3D printed samples (R_2)
1	1, 2, 3
2	4, 5, 6
3	7, 8, 9

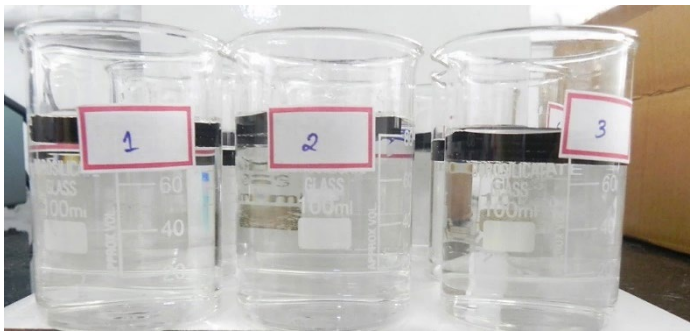

Figure 5. 3D printed specimens immersed in solution

3.0 CHARACTERIZATION TESTS

3.1 Dimensional Accuracy

Dimensional accuracy was determined by measuring 3D printed specimens and comparing them with the CAD models. The measurements were measured using digital vernier calipers (Make: Mitutoyo, 150 mm). Measurements were recorded at three locations (top, middle, bottom sides of the samples) on each of the specimens before and after coating. The error, e of measurements is the difference between the measured value or output value as indicated by V_O and the nominal value or true value as indicated by V_n was calculated using Eq. (1). The error (%) is the absolute error divided by the average value, V_A was calculated by using Eq. (2).

$$\text{Error } (e) = V_O - V_n \tag{1}$$

$$Error(\%) = \left[\frac{Error\ of\ different}{Average}\right] \times 100 \tag{2}$$

3.2 Roughness Determination

The roughness profiles of pre and post coated 3D-printed samples were determined via surface roughness SJ410 profilometer (Make: Mitutoyo, simple column stand). Cut off length λc used in testing was 0.8 mm and sampling length ~5. So total evaluation length, l_m = 0.8 x 5 = 4 mm. 'R_a' is the average roughness attained by computing mean of the deviations from average line artihmetically. Measurements were taken at three different spots and analysed on the surface of each specimen. Roughness values (R_a) were averaged, and observations normalized to the deposition direction. Percentage of deviation in SR before and after coating was calculated by using Eq. (3)[12].

$$Percentage\ of\ deviation = \left[\frac{|Before\ coating\ R_a - After\ coating\ R_a|}{Average}\right] \times 100 \tag{3}$$

3.3 Weight Measurement

Weight of pre and post coated 3D-printed samples were determined via Sartorius weighing balance with precise readability of 0.0001 g. Percentage of increase in weight before and after coating was calculated by using Eq. (4)[12].

$$Deviation\ in\ weight = \left[\frac{|Final\ weight - Initial\ weight|}{Average}\right] \times 100 \tag{4}$$

3.4 Surface Wettability

Wettability of both coated and uncoated samples was gaged utilizing contact angle measurements using a goniometer (DSA25 with temperature-controlled chamber, KRUSS, Germany). The droplets were analysed using KYOWA's FAMAS (Interface Measurement and Analysis System). Drops of 2 µl of liquids were dropped on 3D printed surfaces

via syringe, at a temperature of 20°C. Surface condition was assessed and averaged at 3 droplet angles. Wenzel state develops when a liquid droplet enters the surface asperities, resulting in enhanced contact fractions. Cassie-Baxter state permits the droplets to stick to their pyramidal structures, trapping air at the surface pores, thereby causing very few droplets to contact solid surfaces. Thus spherical droplets roll across the surface and attach to the hydrophobic surface in the Cassie-Baxter condition, shown in Figure 6 [3].

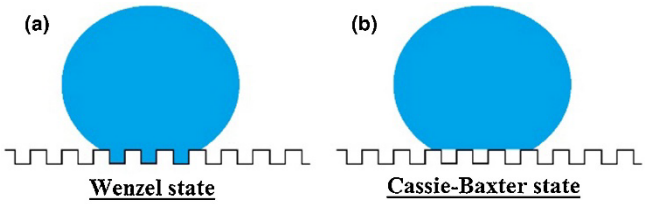

Figure 6. Droplet wettability stages [3]

WCAs between 10° < θ < 90° indicate a hydrophilic regime and those between 90° < θ < 150° indicate a hydrophobic regime. Superhydrophilicity is when the WCA < 10° in less than 1 second from initial wetting. On the other hand, WCAs > 150° indicate super hydrophobicity as shown in Figure 7.

Property	Super hydrophilic	Hydrophilic	Hydrophobic	Super hydrophobic
Drop diagram				
Contact angle	θ < 10°	θ< 90°	θ > 90°	θ > 150°

Figure 7. Water droplet contact angle [28]

3.5 Microstrcture of 3D Printed Samples

Variations in surface morphology with coating treatment were noticed through Field Emission Scanning Electron Microscope (FE SEM). JFC-1100E ion sputtering device was employed for glazing of samples by gold (60 seconds, 10 mA) for obtaining a path for electrons as the polymer has nonconducting character as well as to achieve ample contrast in SEM micrographs.

3.6 Water Absorption

Water absorption capacity of 3D-printed samples pre and post coatings was tested as per ASTM D570 standard. The water absorption tests were executed by soaking the R_1 and R_2 samples in distilled water for different periods of time followed by measurement of weight of the samples. For the first 4 hours, the weight of samples was measured every 30 minutes, and 8 measurements were acquired. Second, the weight of the samples was monitored every 24 hours for the next 3 days, obtaining three measurements. The samples had been immersed in water for 72 hours. After the immersion time, samples were removed from water and weighed. Before immersion in water, dry weight of samples was also recorded. WA capacity was calculated by using Eq. (5) [24].

$$WG = \left[\frac{|W_s - W_d|}{W_d}\right] \times 100\ \% \tag{5}$$

where, W_s is the saturated weight and W_d is the dry weight of the samples.

Porosity of samples were calculated by using Eq. (6), where density of water is 1 g/cm^3 and V is the volume of cube.

$$P = \left[\frac{(m_{sat} - m_{dry}/\rho_{H_2O}}{V}\right] \times 100\ \% \tag{6}$$

$$\left|\frac{WG}{Area} = \frac{m_{wet} - m_{dry}}{A\ x\ m_{dry}}\right| \tag{7}$$

where, A is the area of one of the faces of the specimen, and m_{wet} represents the wet mass of the specimen at a particular instant.

4.0 RESULTS AND DISCUSSION

4.1 Dimensional Accuracy

A summary of the measurements can be found in Table 10. Measurement was taken along three axes, namely x, y, and z, as shown in Figure 8. Based on the comparison, the accuracy of the measurement was evaluated. For comparison purposes, the average value of each printed sample was used as the base value. In order to calculate the error and percentage error, equations 1 and 2 were used.

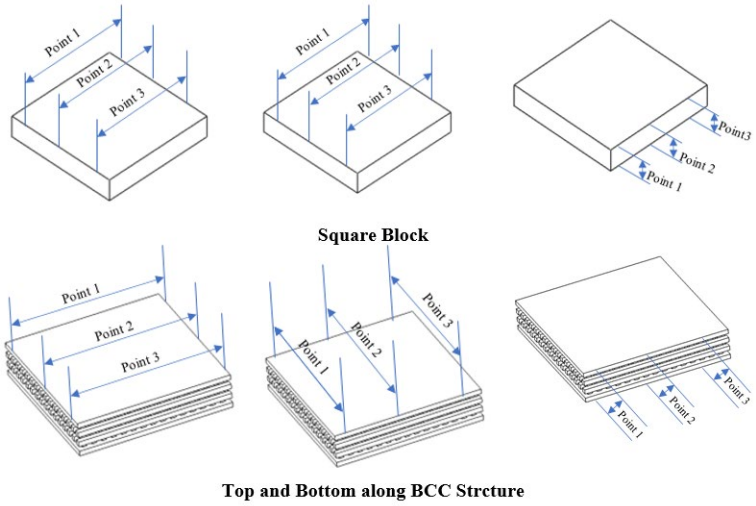

(a) (b) (c)

Figure 8. Measurement positions along axes: (a) x-axis, (b) y-axis and (c) z-axis

With 0.15 mm layer height, the average of measured values for sample 1 are 31.01, 31.02, 5.04 mm, for sample 2 are 31.02, 31.01, 5.01 mm, and for sample 3 are 31.02, 31.02, 7.01mm along x, y, z axes, respectively. With 0.17 mm layer height, the average of measured values for sample 4 are 31.01, 31.02, 5.03 mm, for sample 5 are 31.03, 31.02, 5.05 mm, and sample 6 are 31.01, 31.04, 7.04 mm along x, y, z axes, respectively. With 0.20 mm layer height, the average of measured values for sample 7 are 31.04, 31.02, 5.01 mm, for sample 8 are 31.04, 31.01, 5.03 mm and for sample 9 are 31.06, 31.04, 7.04 mm along x, y, z axes, respectively.

The error plots for DA are shown in Figure 9. For layer height of 0.15 mm, error (%) of 0.043, 0.075, 0.794 for sample 1, error (%) of 0.064, 0.043, 0.200 for sample 2 and error (%) of 0.054, 0.054, 0.190 for sample 3 along x, y, z axes respectively were recorded. For layer height of 0.17 mm, error (%) of 0.032, 0.075, 0.662 for sample 4, error (%) of 0.107, 0.064, 0.990 for sample 5 and error (%) of 0.043, 0.118, 0.521 for sample 6 along x, y, z axes respectively were recorded. For layer height of 0.20 mm, error (%) of 0.140, 0.054, 0.266 for sample 7, error (%) of 0.118, 0.043, 0.662 for sample 8 and error (%) of 0.182, 0.118, 0.615 for sample 9 along x, y, z axes respectively were recorded. Minimal deviation from the nominal dimensions indicates a more precise dimensional measurement of the 3D-printed samples.

Impact of layer height on dimensional accuracy of 3D printed samples has the least significant percentage contribution among other factors investigated in this study. Results of the same are displayed Table 10. There are minimal differences in dimension between coated and uncoated samples due to the ultra-thin coating applied to the specimens as detected using a CMM. Flash Forge 3D printer is known to be the most accurate in terms of accuracy. Improper maintenance of printer might result in samples to have a lower DA. Additionally, the error (%) of a sample can increase naturally as the life of the printer increases, causing the DA to decrease.

Table 10. Error (%) for 3D printed samples

Specimens	Axis	Original values	Measured values			Avg. of measured values	Difference	Error (%)
1	x	31	31	31.01	31.03	31.01	0.01	0.043
	y	31	31.03	31.01	31.03	31.02	0.02	0.075
	z	5	5.03	5.04	5.05	5.04	0.04	0.794
2	x	31	31.03	31.02	31.01	31.02	0.02	0.064
	y	31	31.01	31.01	31.02	31.01	0.01	0.043
	z	5	5	5.02	5.01	5.01	0.01	0.200

Table 10. (cont.)

Specimens	Axis	Original values	Measured values			Avg. of measured values	Difference	Error (%)
3	x	31	31.01	31.02	31.02	31.02	0.02	0.054
	y	31	31.01	31.03	31.01	31.02	0.02	0.054
	z	7	7.01	7.01	7.02	7.01	0.01	0.190
4	x	31	31	31.02	31.01	31.01	0.01	0.032
	y	31	31.05	31.02	31	31.02	0.02	0.075
	z	5	5.02	5.03	5.05	5.03	0.03	0.662
5	x	31	31.01	31.04	31.05	31.03	0.03	0.107
	y	31	31	31.03	31.03	31.02	0.02	0.064
	z	5	5.05	5.06	5.04	5.05	0.05	0.990
6	x	31	31.01	31.02	31.01	31.01	0.01	0.043
	y	31	31.04	31.03	31.04	31.04	0.04	0.118
	z	7	7.05	7.02	7.04	7.04	0.04	0.521
7	x	31	31.04	31.05	31.04	31.04	0.04	0.140
	y	31	31.02	31.01	31.02	31.02	0.02	0.054
	z	5	5.03	5	5.01	5.01	0.01	0.266
8	x	31	31.03	31.05	31.03	31.04	0.04	0.118
	y	31	31	31.02	31.02	31.01	0.01	0.043
	z	5	5.04	5.02	5.04	5.03	0.03	0.662
9	x	31	31.05	31.07	31.05	31.06	0.06	0.182
	y	31	31.03	31.06	31.02	31.04	0.04	0.118
	z	7	7.04	7.05	7.04	7.04	0.04	0.615

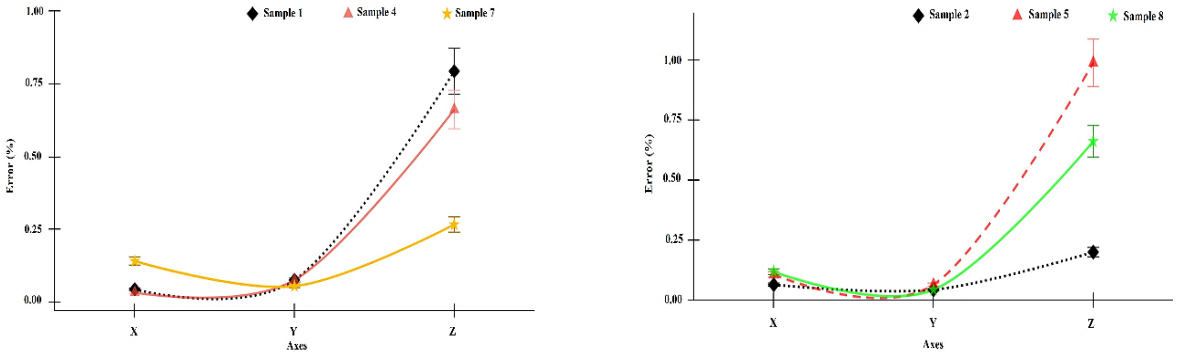

(a)

(b)

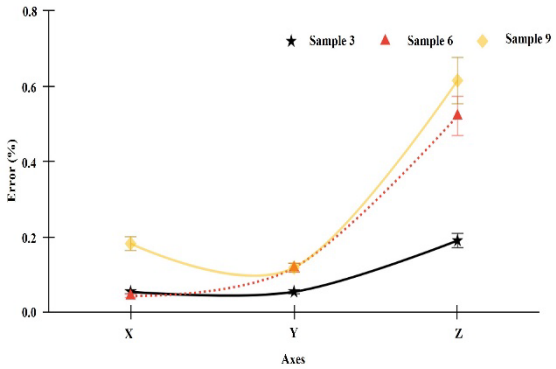

(c)

Figure 9. Error (%) plots along axes: (a) BCC structure, (b) square block and (c) top and bottom plates along the structure

4.2 Surface Roughness

Surface roughness (SR) is investigated to know the impact of printing parameters pre and post coating. Table 11 summarizes the average R_a values before and after coating for each printing parameter. Percentage of deviation was calculated by using Eq. (3). The average surface roughness ranged between 2.275 and 6.923 µm for R_1 samples and for R_2 samples it ranged from 2.077 to 5.553 µm. Figure 11 reveals 2D roughness profiles of 3D printed R_1 and R_2 samples. For the coated sample 2 with layer height of 0.15 m, R_a value decreased from 2.809 to 2.077 µm, resulting in a 29.96% reduction in SR. Sample 3 had a R_a value of 4.923 µm, which was reduced to 4.553 µm. Sample 5 with layer height of 0.17 mm had a R_a value of 2.975 µm, which was reduced to 2.188 µm after coating. In sample 6, R_a before the coating was 5.323 µm which was reduced to 3.428 µm after coating. In correlation to 0.20 mm layer height, R_a value for sample 8 reduced from 3.557 to 2.809 µm after coating i.e., a reduction of 23.50%. In sample 9, roughness reduced by 21.96% before coating from 6.923 µm to 5.553 µm.

Table 11 and Figure 10 illustrate the results of SR. Figure 10 shows that the SR of samples after coating was significantly reduced. Highest R_a of 6.923 µm was seen in sample 9 with layer height of 0.20 mm, and lowest R_a of 2.809 µm was noted in sample 2 with layer height of 0.15 mm. Sample 2 exhibited lowest R_a of 2.077 µm whereas sample 9 highest R_a of 5.553 µm which could be attributed to the application of coating on these samples. Prior to coating, specimens showed higher peak points and more fluctuations. Post-coating, the peak heights of the 3D printed samples are significantly reduced, resulting in a smoother surface. As presented in Figure 11(b), SR decreased due to the application of coating. In consequence, high SR will affect hydrophobic performance. As depicted in Figure 10, layer thickness and filling method apparently affected 3D printed surface roughness. When other parameters remain constant, a rise in layer thickness leads to an increase in surface roughness.

Table 11. Average R_a values for before and after coating of 3D printed samples

Samples	Average R_a		Deviation (%)
	Before coating (µm)	After coating (µm)	
2	2.809	2.077	29.96
3	4.923	4.553	7.81
5	2.975	2.188	3.90
6	5.323	3.428	43.31
8	3.557	2.809	23.50
9	6.923	5.553	21.96

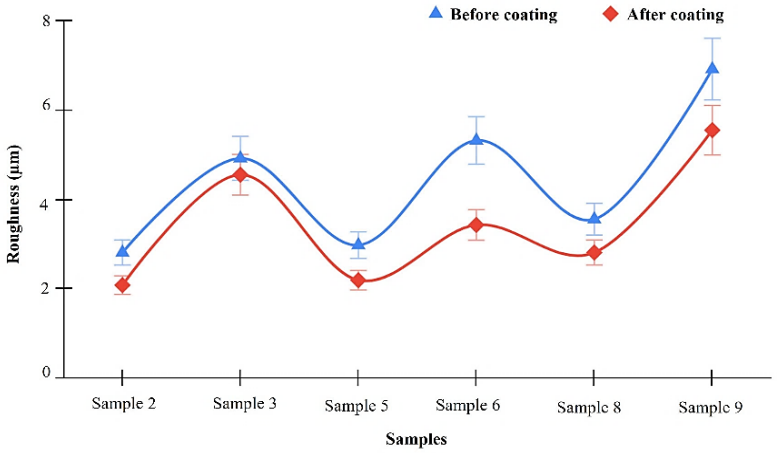

Figure 10. Mean R_a of 3D printed samples pre and post coating

(a)

Figure 11. Roughness profile in 3D printed samples: (a) pre-coating

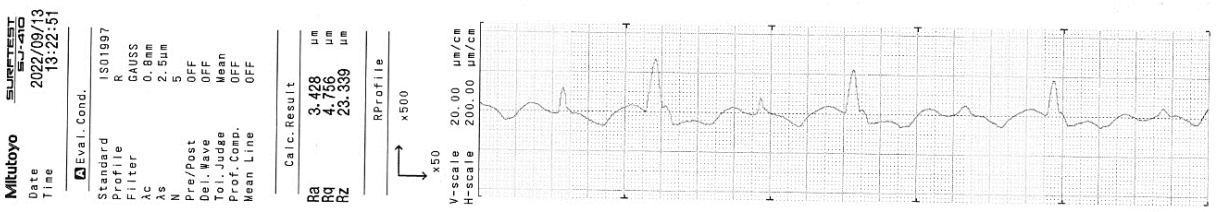

(b)

Figure 11. (cont.) (b) post-coating

4.3 Mass Analysis

In the case of weight analysis, Table 12 summarizes the results, and a graphical representation of mean weight of 3D printed samples R_1 and R_2 before and after coating is exhibited in Figure 12. Pre and post-coating weights were measured for each printed sample. As a result of coating, the samples were heavier. A weight increase of less than 6 % was observed. There was a weight difference of 0.108 g between sample 1 before and after coating with a weight percentage of 4.93 %. A weight difference of 0.005 g separated coated from uncoated samples in sample 2, which increased by 0.21 % in percentage. Among the treated and untreated samples, sample 3 exhibited a weight gain of 3.009 % and a difference of 0.12 g. Sample 4 exhibited 4.426 % WI with a difference of 0.095 g. Sample 5 exhibited 0.497 % WI with a difference of 0.012 g. Sample 6 exhibited 2.645 % WI with a difference of 0.107 g. Sample 7 exhibited 5.852 % WI with a difference of 0.125 g. The difference between uncoated and coated samples of 8 % WI was 0.09%, and the difference between coated and uncoated samples of 9 % WI was 0.167%.

Table 12. Percentage of increase in weight for R_1 and R_2 samples

	Samples								
	1	2	3	4	5	6	7	8	9
Weight before coating (g)	2.192	2.331	3.987	2.146	2.414	4.045	2.136	2.423	4.257
Weight after coating (g)	2.3	2.336	4.107	2.241	2.426	4.152	2.261	2.513	4.42
Percentage of increase (%)	4.93	0.21	3.009	4.426	0.497	2.645	5.852	3.714	3.829
Difference (g)	0.108	0.005	0.12	0.095	0.012	0.107	0.125	0.09	0.163

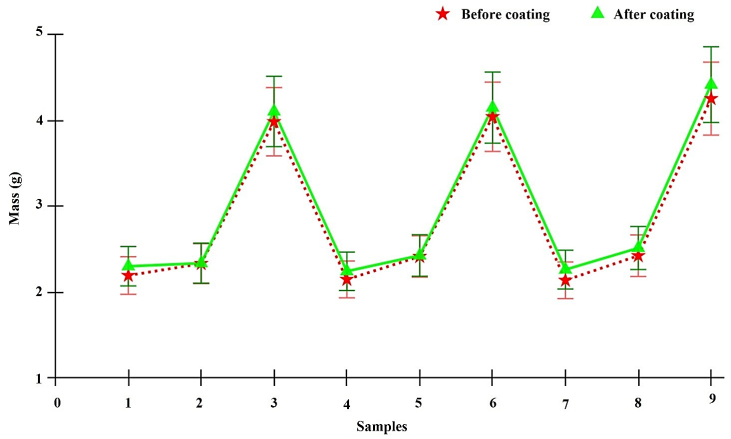

Figure 12. Mean weight of 3D printed samples pre and post coating

4.4 SEM Analysis

Surface morphology investigation was carried out on coated and uncoated samples. As depicted in Figure 13, FE SEM illustrations of samples were studied to determine the morphology of coated and uncoated samples. Post coating, the flat printed samples exhibited a roughness of 2 µm - 5 µm, which is a characteristic of FDM 3D printing filament. The roughness of printed surface indicate anisotropy depending on the direction of printing. A variety of magnification powers were selected in order to compare SEM images. It was observed that the X-Y plane of the printer marks had tiny pits located at a constant distance from each other. During the printing process, the printing head moves, causing these marks.

4.5 Surface Wettability

Variation in contact angle between 3D-printed coated and uncoated samples is depicted in Table 13. Sessile drop methodology was employed in determining the contact angle, which indicated surface hydrophobicity. A comparison was made between coated and uncoated samples. The hydrophilic property of all samples was turned into a hydrophobic

property after coating. WCA plots for R_1 and R_2 samples are depicted graphically in Figure 15. WCA measured on the coated surface of sample 1 was 139.2°, indicating a higher CA i.e., 45.3° than on the uncoated surface. For sample 2, WCA measured for the uncoated sample was 84.4° to 127.6° after coating the sample. Both uncoated and coated samples for sample 3 had contact angles ranging from 79.3° to 122.5°. In sample 4, WCA measured on the coated surface was 130.8°, indicating a higher CA i.e., 36° than on the uncoated surface. In sample 5, the uncoated sample exhibited WCA of 88.3°, and the coated sample 108.7°. In sample 6, the CA increased from 83.3° to 119.5° after coating. For sample 7, WCA before and after coating was 95.1° & 118.6°. When comparing uncoated and coated samples, the range was 71.9° to 103.4° for sample 8 and 84.9° to 117.9° for sample 9. According to the results of WCA, the same coatings were applied to samples printed under different process parameters in order to achieve the same surface hydrophobic properties.

Table 13. Droplet angle of 3D printed coated and uncoated samples

	Samples								
	1	2	3	4	5	6	7	8	9
WCA before coating (°)	93.9	84.4	79.3	94.8	88.3	83.3	95.1	71.9	84.9
WCA after coating (°)	139.2	127.6	122.5	130.8	108.7	119.5	118.6	103.4	117.9

4.6 Water Absorption

Water absorption test results for coated and uncoated samples are summarized in Table 14. Various time periods were used to determine how much water could be absorbed by the samples when immersed in distilled water. Weight gain per area and open porosity of 3D printed samples were calculated using Eqs. (5) – (7) by measuring the weight of samples at different time intervals. After coating samples, their water absorption capacity decreased.

Table 14. Water absorption results for coated and uncoated samples

Sample Number	Before coating			After coating		
	WG (%)	P	WG/A	WG (%)	P	WG/A
1	64.83	0.029574	0.003241	45.46	0.021759	0.002502
2	11.71	0.005810	0.000081	6.93	0.003370	0.000394
3	35.18	0.020848	0.005819	27.14	0.016568	0.004763
4	60.98	0.027233	0.002922	49.98	0.023311	0.002612
5	10.75	0.005400	0.000678	7.20	0.003537	0.000442
6	34.08	0.020495	0.005803	25.61	0.015804	0.004593
7	58.93	0.026195	0.002798	51.86	0.023052	0.002462
8	12.95	0.006529	0.000791	7.94	0.004137	0.000488
9	29.91	0.019063	0.005641	24.22	0.015329	0.004568

SEM images of 3D printed samples indicate minimal porosity on the printed lines as compared to coated and uncoated samples. Figure 13(ii) shows BCC structure (a-c), square block (d-f), and top and bottom plates along the structure (g-i) on coated samples. However, some minor porosity was observed due to the presence of tricalcium phosphate and chitin coating content. 3D printed bodies consist of lines that form layers. As seen in uncoated samples of Figure 13(i), the lines from printing are relatively consistent in diameter. Observations reveal rough surfaces and a lack of fusion between successive layers. Waviness might be caused by unfused layers of material due to which surfaces that are coated or uncoated have relatively higher roughness.

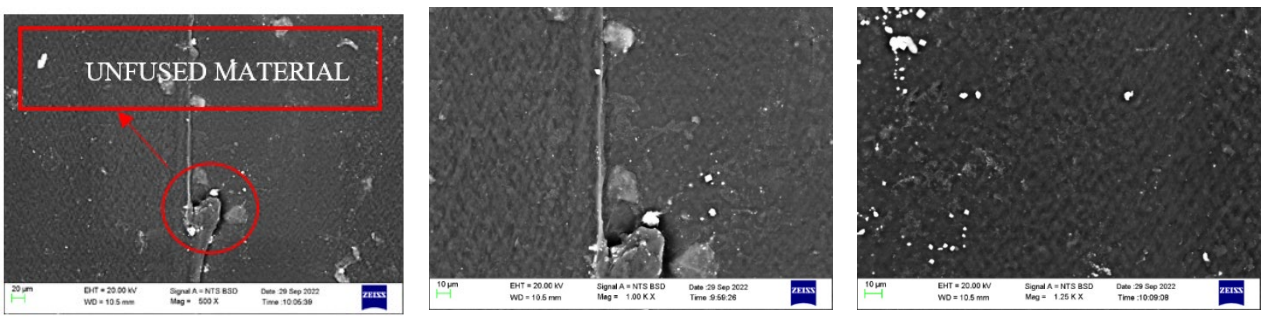

(a) (b) (c)

Uncoated samples

Figure 13. SEM images of different magnifications

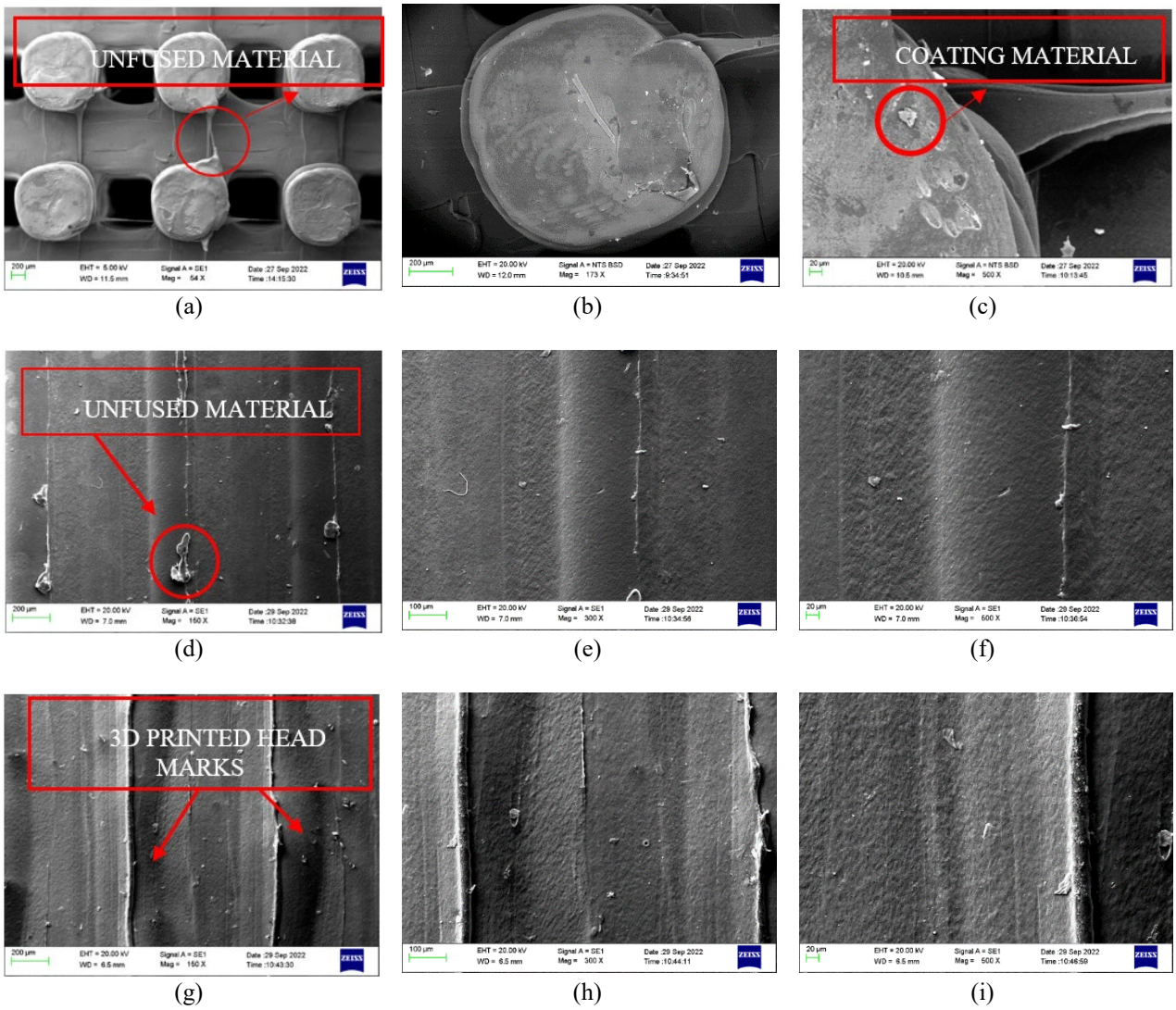

(a) (b) (c)

(d) (e) (f)

(g) (h) (i)

(ii) Coated samples

Figure 13. (cont.)

3D printed coated and uncoated samples were evaluated for hydrophobicity based on the coating preparation and WCA measurement methods. The results are shown in Figure 14 and 15. WCA at 0.15 mm layer height was 139.2° and 103.4° at 0.20 mm layer height. Prior to coating, WCA at 0.15 mm layer height was 93.9°, and 71.9° at 0.20 mm layer height. Hydrophobic performance was found to be affected by process parameters. A tricalcium phosphate-chitin solution coating with immersion technique increased the hydrophobicity of 3D printed ABS samples. The hydrophobic performance of a layer was greatly affected by its layer height.

The results of water absorption are listed in Table 14, and weight gain plots are shown in Figure 16. Prior to coating, sample 1 had the highest weight gain of 64.83 % and sample 5 had the lowest weight gain of 10.75%. Weight gain after coating was lowest in sample 2 at 6.93 % and highest in sample 7 at 51.86%. A plot of the open porosity error is shown in Figure 17. Results indicate influence of process parameters on water absorption rate. A high absorption rate was observed before coating, while low absorption rate after coating. Dip coating of ABS parts effectively protected WA from damage. Polymers can also form microcracks when they are processed at high temperatures. Increase of micro-cracks may result in absorption of water. This process can be used to create many different functional hydrophobic 3D products with low water adhesion and liquid position control.

Uncoated Samples Coated Samples

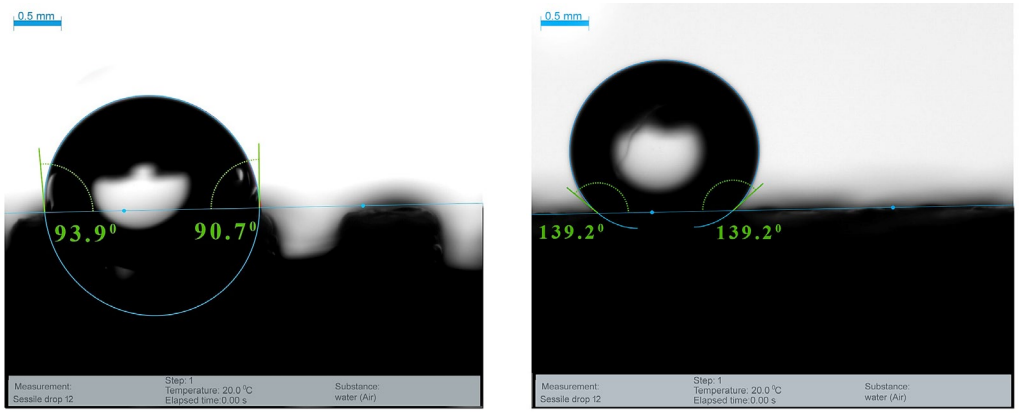

(a)

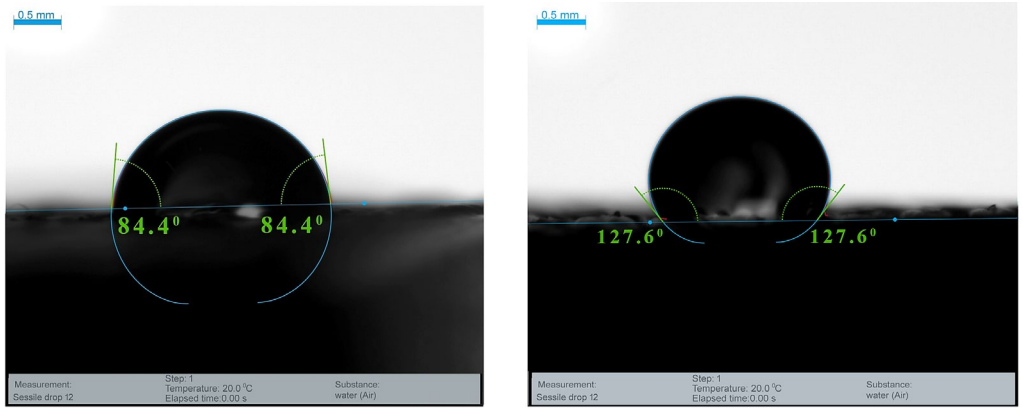

(b)

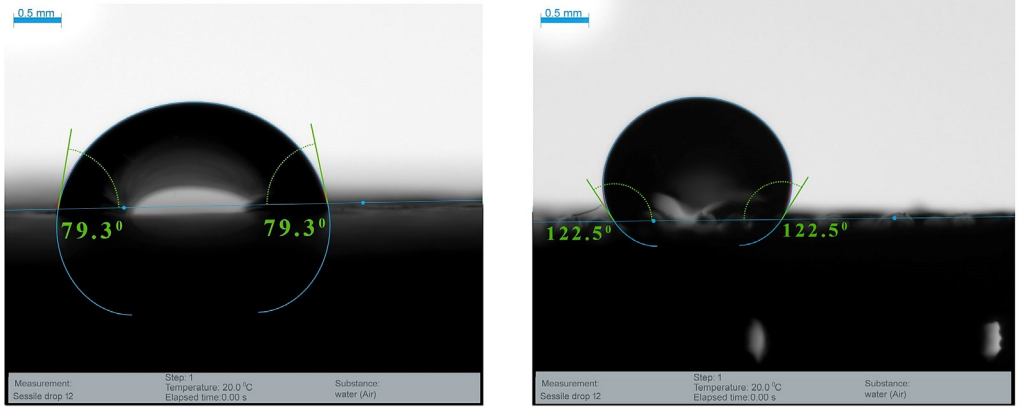

(c)

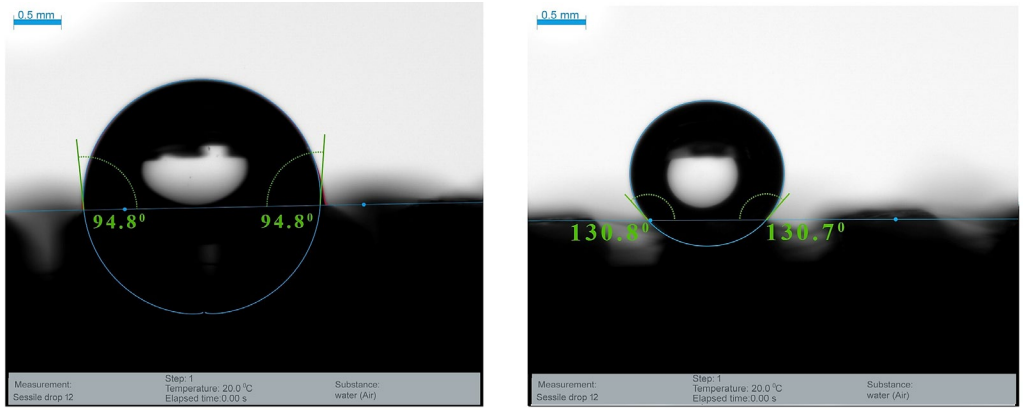

(d)

Figure 14. WCA in coated and uncoated samples: (a) sample 1, (b) sample 2, (c) sample 3, (d) sample 4

Uncoated Samples Coated Samples

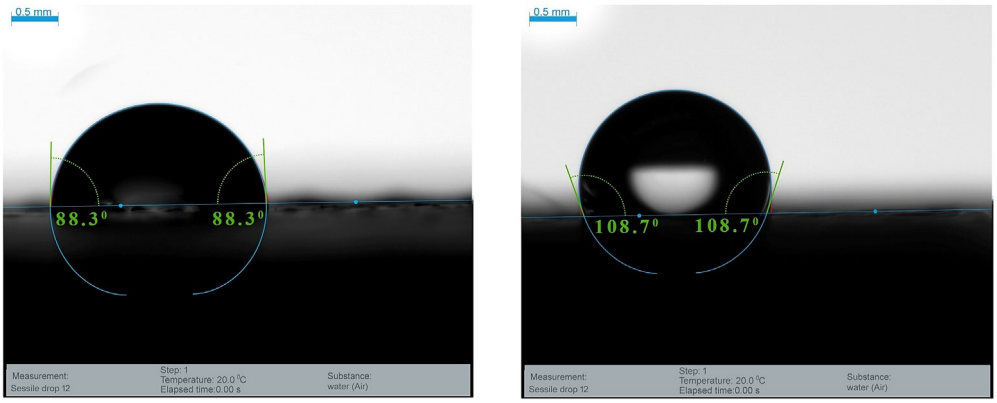

(e)

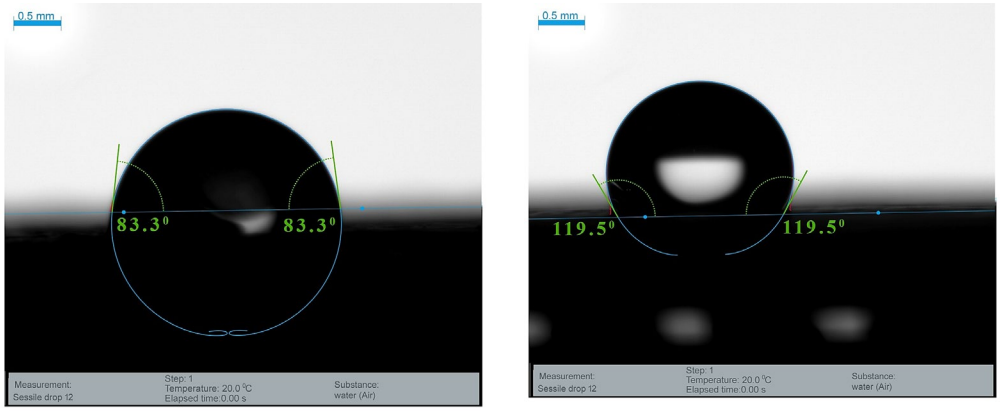

(f)

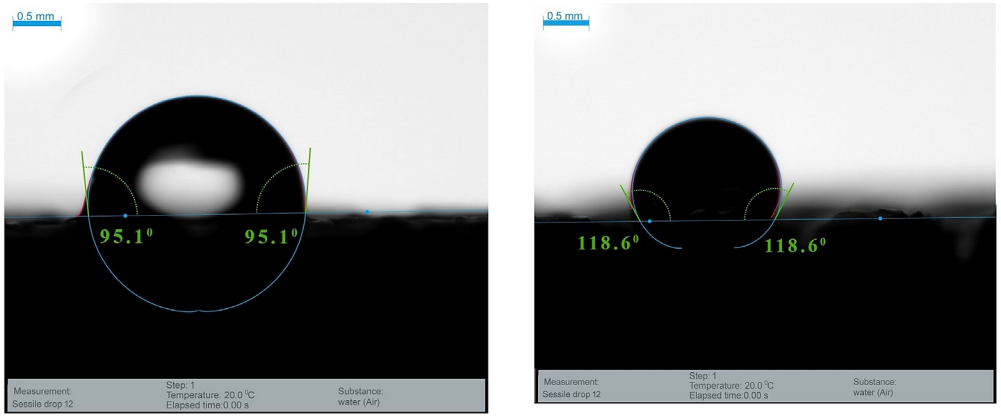

(g)

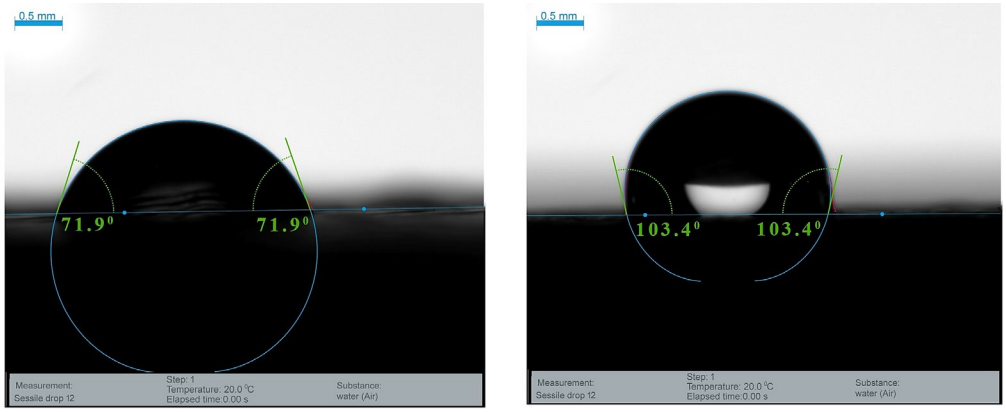

(h)

Figure 14. (cont.) (e) sample 5, (f) sample 6, (g) sample 7, (h) sample 8

Uncoated Samples | Coated Samples

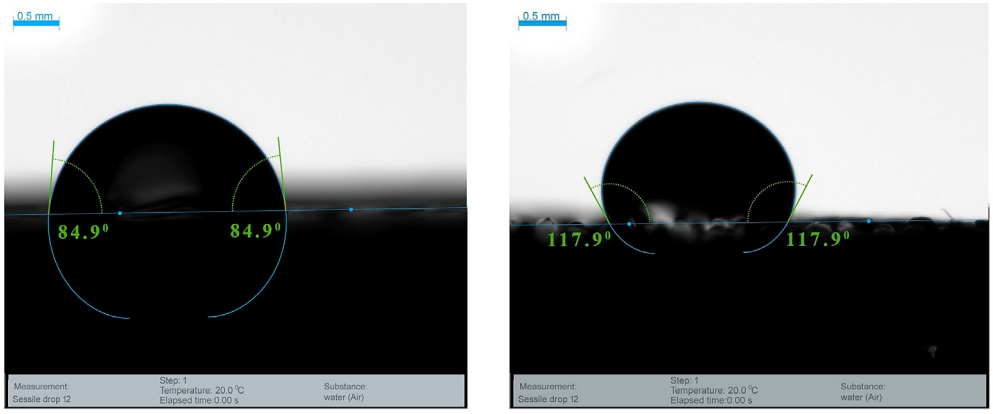

(i)

Figure 14. (cont.) (i) sample 9

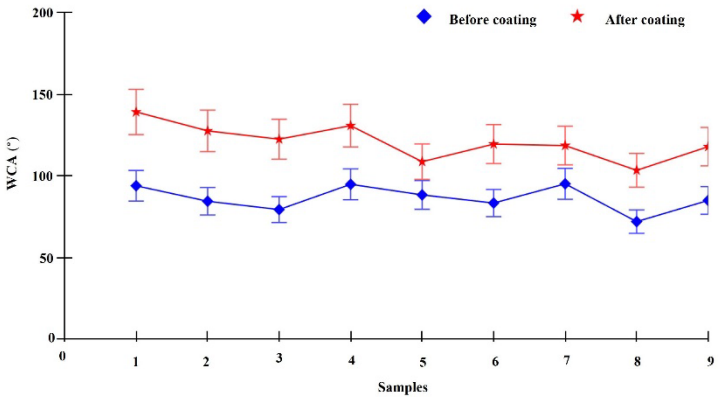

Figure 15. WCA plots for R_1 and R_2 samples

Before Coating | After Coating

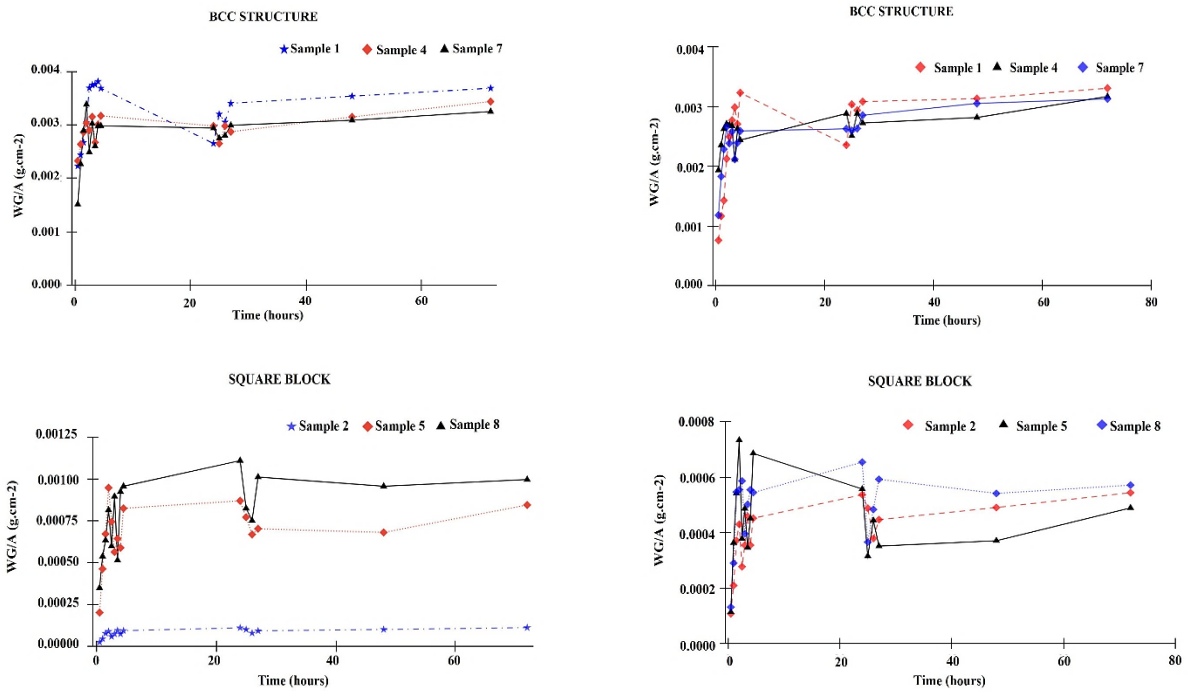

Figure 16. Evaluation of weight gain per area on 3D printed R_1 and R_2 samples

Before Coating | After Coating

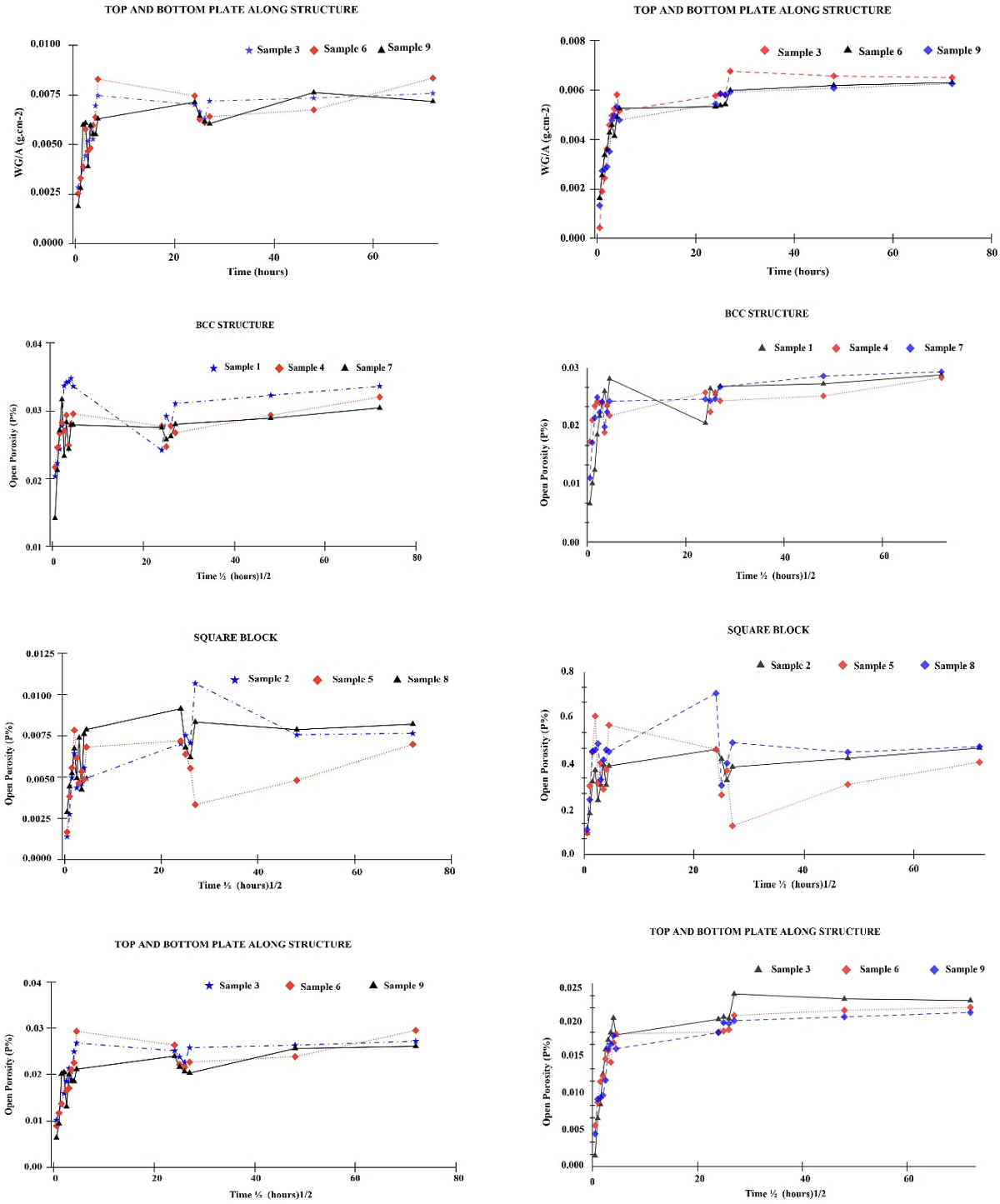

Figure 17. Evolution of open porosity of 3D-printed samples pre and post coating

5.0 CONCLUSIONS

Experimental studies were accomplished for surface characterization on coated and bare 3D-printed ABS samples by controlling layer height and infill percentage variables. Hydrophobic clear solution was synthesized using tricalcium phosphate and chitin clear solution in a 70:30 ratio that was successful in developing hydrophobic solutions. The dip coating process was successful in creating a hydrophobic coating, thereby improving the hydrophobicity of ABS specimens. Because the specimens were coated with an ultra-thin layer, they differ in dimensions slightly from the uncoated samples. With an increase in layer thickness, surface roughness was found to increase. SEM pictures exhibited interlayer bonding of the fabricated parts was superior to those of the other parts. Uncoated samples had a WCA of 90° or less, which indicate hydrophilic properties, but after coating they had a WCA of over 100°, indicating hydrophobic nature. The CA decreased with layer thickness; samples at 0.15 mm had the highest CA of over 139.2°. After dip coating, ABS parts were effectively protected from WA compared to uncoated samples. Hydrophobicity of layer was found to be

greatly impacted by layer height. A similar topic could be explored in future research, including monitoring the properties of surfaces during periods of weathering or any other kind of influence.

6.0 ACKNOWLEDGMENTS

This study was not supported by any grants from funding bodies in the public, private or not-for-profit sectors. Acknowledgements are due to VNRVJIET for providing the ncessary resources for carrying out the research work and DMRL Hyderabad for their help in SEM analysis. Support provided by the staff of Additive Manufacturing laboratory, Chemistry Laboratory, Center for Nanotchnology, VNRVJIET and ARCI Hyderabad are appreciated.

7.0 ABBREVIATIONS

ABS	Acrylonitrile Butadiene Styrene
AT	Alkali Treatment
CA	Contact Angle
(C8H13O5N)n	Chitin
Ca3(PO4)2	Tricalcium Phosphate
CMM	Coordinate Measuring Machine
DA	Dimensional Accuracy
DMAc	N-Dimethylacetamide
DOE	Design of Experiments
FDM	Fused Deposition Modeling
FE SEM	Field Emission Scanning Electron Microscope
HCl	Hydrochloric Acid
LiCl	Lithium Chloride
LT	Layer Thickness
MEk	Methyl Ethyl ketone
NaOH	Sodium Hydroxide
nHA	Nano Hydroxyapatite
OA	Orthogonal Array
R1	Uncoated Samples
R2	Coated Samples
RA	Raster Angle
Ra	Average Roughness
SE	Surface Energy
SEM	Scanning Electron Microscope
SR	Surface Roughness
WA	Water Absorption
WCA	Water Contact Angle
WI	Weight Increase

8.0 REFERENCES

[1] V. G. Gokhare, D. N. Raut, and D. K. Shinde, "A review paper on 3D-printing aspects and various processes used in the 3D-printing," *International Journal of Engineering Research & Technology*, vol. 6, no. 6, pp. 953–958, 2017.

[2] T. D. Ngo, A. Kashani, G. Imbalzano, K. T. Q. Nguyen, and D. Hui, "Additive manufacturing (3D printing): A review of materials, methods, applications and challenges," *Composites Part B: Engineering*, vol. 143, pp. 172–196, 2018.

[3] S. Poornaganti, S. N. Yeole, and J. P. Kode, "Insights on surface characterization of 3D printed polymeric parts," *Materials Today: Proceedings*, vol. 62, pp. 3837–3848, 2022.

[4] K.-M. Lee, H. Park, J. Kim, and D.-M. Chun, "Fabrication of a superhydrophobic surface using a fused deposition modeling (FDM) 3D printer with poly lactic acid (PLA) filament and dip coating with silica nanoparticles," *Applied Surface Science*, vol. 467–468, pp. 979–991, 2019.

[5] R. Chand, V. S. Sharma, R. Trehan, M. K. Gupta, and M. Sarikaya, "Investigating the dimensional accuracy and surface roughness for 3D printed parts using a multi-jet printer," *Journal of Materials Engineering and Performance*, vol. 32, no. 3, pp. 1145–1159, 2023.

[6] G. S. Robles, R. N. M. Delda, R. L. B. Del Rosario, M. T. Espino, and J. R. C. Dizon, "Dimensional accuracy of 3D-printed acrylonitrile butadiene styrene: effect of size, layer thickness, and infill density," in *Key Engineering Materials*, vol. 913, pp. 17–25, 2022.

[7] S. R. Pradhan, R. Singh, S. S. Banwait, M. S. Puhal, S. Singh, and A. Anand, "A comparative study on investment casting of dental crowns for veterinary dentistry by using ABS patterns with and without wax coating," in *E3S Web of Conferences*, vol. 309, p. 01020, 2021.

[8] A. Mura, F. Adamo, H. Wang, W. S. Leong, X. Ji, and J. Kong, "Investigation about tribological behavior of ABS and PC-ABS polymers coated with graphene," *Tribology International*, vol. 134, pp. 335–340, 2019.

[9] W. Chen *et al.*, "Alkali treatment facilitates functional nano-hydroxyapatite coating of 3D printed polylactic acid scaffolds," *Materials Science and Engineering: C Materials for Biological Applications*, vol. 120, p. 111686, 2021.

[10] P. Kowalczyk, P. Trzaskowska, I. Łojszczyk, R. Podgórski, and T. Ciach, "Production of 3D printed polylactide scaffolds with surface grafted hydrogel coatings," *Colloids and Surfaces B: Biointerfaces*, vol. 179, pp. 136–142, 2019.

[11] V. Pestano, M. Pohlmann, and F. P. da Silva, "Effect of acetone vapor smoothing process on surface finish and geometric accuracy of fused deposition modeling ABS parts," *Journal of Materials Science and Chemical Engineering*, vol. 10, no. 10, pp. 1–9, 2022.

[12] J. S. Chohan *et al.*, "Taguchi S/N and TOPSIS based optimization of fused deposition modelling and vapor finishing process for manufacturing of ABS plastic parts," *Materials*, vol. 13, no. 22, p. 5176, 2020.

[13] M. R. Khosravani, J. Schüürmann, F. Berto, and T. Reinicke, "On the post-processing of 3D-printed ABS parts," *Polymers*, vol. 13, no. 10, p. 1559, 2021.

[14] M. F. M. Omar, S. Sharif, M. Ibrahim, H. Hehsan, M. N. M. Busari, and M. N. Hafsa, "Evaluation of direct rapid prototyping pattern for investment casting," *Advanced Materials Research*, vol. 463–464, pp. 226–233, 2012.

[15] A. Haidiezul, A. Aiman, and B. Bakar, "Surface finish effects using coating method on 3D printing (FDM) parts," in *IOP Conference Series: Materials Science and Engineering*, vol. 318, p. 012065, 2018.

[16] J. Sierra, D. Sanín, A. Montoya, and W. Villaneda, "Relation between mechanical properties and 3D printer configurations parameters using PLA at open-source prusa i3," *International Journal of Integrated Engineering*, vol. 12, no. 8, 2020.

[17] Y. Chai, R. W. Li, D. M. Perriman, S. Chen, Q. H. Qin, and P. N. Smith, "Laser polishing of thermoplastics fabricated using fused deposition modelling," *The International Journal of Advanced Manufacturing Technology*, vol. 96, no. 9–12, pp. 4295–4302, 2018.

[18] A. Garg, A. Bhattacharya, and A. Batish, "Chemical vapor treatment of ABS parts built by FDM: Analysis of surface finish and mechanical strength," *The International Journal of Advanced Manufacturing Technology*, vol. 89, no. 5–8, pp. 2175–2191, 2017.

[19] N. Encinas, M. Pantoja, J. Abenojar, and M. A. Martínez, "Control of wettability of polymers by surface roughness modification," *Journal of Adhesion Science and Technology*, vol. 24, no. 11–12, pp. 1869–1883, 2010.

[20] B. Kang, J. Hyeon, and H. So, "Facile microfabrication of 3-dimensional (3D) hydrophobic polymer surfaces using 3D printing technology," *Applied Surface Science*, vol. 499, p. 143733, 2020.

[21] H. M. Ali, M. A. Qasim, S. Malik, and G. Murtaza, "Techniques for the fabrication of super-hydrophobic surfaces and their heat transfer applications," in *Heat Transfer - Models, Methods and Applications*, InTech, 2018.

[22] Z. Wang, L. Yuan, G. Liang, and A. Gu, "Mechanically durable and self-healing super-hydrophobic coating with hierarchically structured KH570 modified SiO_2-decorated aligned carbon nanotube bundles," *Chemical Engineering Journal*, vol. 408, p. 127263, 2021.

[23] M. S. Hasan, T. Ivanov, D. Tanovic, A. Simonovic, and M. Vorkapic, "Dimensional accuracy and experimental investigation on tensile behavior of various 3D printed materials," in *9th International Scientific Conference on Defensive Technologies, OTEH 2020*, Belgrade, Serbia, 2020, pp. 400–406.

[24] C. Vicente, J. Fernandes, A. Deus, M. Vaz, M. Leite, and L. Reis, "Effect of protective coatings on the water absorption and mechanical properties of 3D printed PLA," *Frattura ed Integrità Strutturale*, vol. 13, no. 48, pp. 748–756, 2019.

[25] K.-E. Aslani, K. Kitsakis, J. D. Kechagias, N. M. Vaxevanidis, and D. E. Manolakos, "On the application of grey Taguchi method for benchmarking the dimensional accuracy of the PLA fused filament fabrication process," *SN Applied Sciences*, vol. 2, no. 6, p. 1016, 2020.

[26] Z. I. Tarmizi *et al.*, "Fabrication of hydrophilic silica coating varnish on pineapple peel fiber based biocomposite," *International Journal of Integrated Engineering*, vol. 11, no. 7, pp. 77–82, 2019.

[27] V. Queral, E. Rincón, V. Mirones, L. Rios, and S. Cabrera, "Dimensional accuracy of additively manufactured structures for modular coil windings of stellarators," *Fusion Engineering and Design*, vol. 124, pp. 173–178, 2017.

[28] V. Lovinčić Milovanović, C. Guyon, I. Grčić, M. Tatoulian, and D. Vrsaljko, "Modification of surface hydrophobicity of PLA/PE and ABS/PE polymer blends by ICP etching and CF_x coating," *Materials*, vol. 13, no. 23, p. 5578, 2020.

[29] K. D. Nguyen and T. Kobayashi, "Chitin hydrogels prepared at various lithium chloride/n,n-dimethylacetamide solutions by water vapor-induced phase inversion," *Journal of Chemistry*, vol. 2020, pp. 1–16, 2020.

[30] S. Wang, J. Sha, W. Wang, C. Qin, W. Li, and C. Qin, "Superhydrophobic surfaces generated by one-pot spray-coating of chitosan-based nanoparticles," *Carbohydrate Polymers*, vol. 195, pp. 39–44, 2018.

[31] A. Beganskiene *et al.*, "Sol-gel approach to the calcium phosphate nanocomposites," in *Nanostructured Materials and Nanotechnology VII*, vol. 34, pp. 1–13, 2013.

[32] B. Barraza *et al.*, "Superhydrophobic SLA 3D printed materials modified with nanoparticles biomimicking the hierarchical structure of a rice leaf," *Science and Technology of Advanced Materials*, vol. 23, no. 1, pp. 300–321, 2022.

[33] B. Du *et al.*, "Superhydrophobic surfaces with pH-induced switchable wettability for oil–water separation," *ACS Omega*, vol. 4, no. 15, pp. 16508–16516, 2019.

[34] P. Dimitrakellis and E. Gogolides, "Hydrophobic and superhydrophobic surfaces fabricated using atmospheric pressure cold plasma technology: A review," *Advances in Colloid and Interface Science*, vol. 254, pp. 1–21, 2018.

[35] M. Schneider, C. Günter, and A. Taubert, "Co-deposition of a hydrogel/calcium phosphate hybrid layer on 3D printed poly (lactic acid) scaffolds via dip coating: towards automated biomaterials fabrication," *Polymers*, vol. 10, no. 3, pp. 275, 2018.

[36] D. Moreno Nieto, M. Alonso-García, M.-A. Pardo-Vicente, and L. Rodríguez-Parada, "Product design by additive manufacturing for water environments: study of degradation and absorption behavior of PLA and PETG," *Polymers*, vol. 13, no. 7, pp. 1036, 2021.